J. Fluid Mech. (1973), *vol.* 61, *part* 1, *pp.* 33–63
Printed in Great Britain

Measurements in a self-preserving plane wall jet in a positive pressure gradient

By H. P. A. H. IRWIN
Department of Mechanical Engineering, McGill University, Montreal, Canada

(Received 3 April 1973)

Measurements of a wall jet in a self-preserving pressure gradient are described. The quantities measured with a linearized hot-wire anemometer were the mean velocity, the turbulence stresses, triple and quadruple velocity correlations, intermittency and spectra of the longitudinal turbulence intensity. The turbulence, as well as the mean flow, reached a self-preserving state in which the ratio of the maximum velocity to the free-stream velocity was 2·65. Skin friction was also measured using the razor-blade technique in the viscous sublayer and buffer region. The values of the constants in the logarithmic law of the wall are found to be similar to those in boundary-layer and pipe flows. The skin-friction coefficient is slightly lower than that found for the wall jet in still air (Guitton 1970), but close to the formula of Bradshaw & Gee (1962) for the wall jet in an external stream with zero pressure gradient.

A balance of the terms in the turbulence energy equation is presented and discussed. The shearing stress is not zero at the point of maximum velocity but is of opposite sign to that at the wall and hence the contribution of this stress to turbulence production is negative in the outer part of the boundary-layer region. However, the total turbulence production remains positive because the contribution of the normal stresses is positive and slightly larger. The pressure–velocity gradient correlations are evaluated by difference from the Reynolds stress equations and are compared with the theoretical model of Hanjalić & Launder (1972*b*). Agreement is quite good in the outer region of the wall jet. The above model is also compared with the triple velocity correlations and again found to be in fair agreement.

1. Introduction

The experiments described in this paper are concerned with a plane wall jet advancing into an adverse pressure gradient. Wall jets in an external stream have been studied on a number of occasions and stimulus for this research has been the usefulness of a wall jet as a means of preventing boundary-layer separation. Possibly because of the practical implications much, although not all, of this research has been primarily aimed at developing empirical prediction methods and, as a result, there are not many instances where detailed turbulence measurements have been obtained. In the present work a particular case has been studied in detail experimentally with a view to providing more definitive data than has hitherto been available.

Under certain conditions the boundary-layer equations can be reduced to ordinary differential equations and, following Townsend (1956*a*, *b*), flows for which this occurs have been termed self-preserving. The conditions for self-preservation of turbulent wall jets in adverse pressure gradients were first given by Patel & Newman (1961), who assumed that the skin friction could be ignored. When the skin friction is ignored the conditions become similar to those for free jets, which have been dealt with in detail, along with wakes, by Newman (1967) and Gartshore & Newman (1969). For self-preserving flows the interpretation of experimental data and the development of theoretical models become greatly simplified, and Patel (1962) and Gartshore (1965) exploited this in work on wall jets in adverse pressure gradients. A similar course has been followed in the present work, the pressure gradient being tailored to satisfy the conditions for self-preservation, which now include the effect of the skin friction.

The measurements in the present experiments include the skin friction, mean velocity profiles, turbulence shear stress and intensities, spectra, dissipation rate, single-point triple and quadruple velocity correlations and the intermittency. Using the data the terms in the equation for the kinetic energy of the turbulence with the exception of the pressure–*velocity* correlation are evaluated. The pressure–*velocity gradient* correlations are obtained by difference from the Reynolds stress equations assuming, in addition, that the flow is locally isotropic. The pressure–*velocity gradient* correlations and the triple velocity correlations are compared with the model proposed by Hanjalić & Launder (1972*b*).

The measurements of the mean velocity near to the wall, which were made using a linearized hot-wire anemometer, show that the conventional logarithmic law found in boundary-layer and pipe flows applies. This is consistent with the conclusion of Guitton (1970) for the wall jet in still air at a similar Reynolds number. The skin-friction measurements are found to be quite well predicted by the formula proposed by Bradshaw & Gee (1962), which was based on their data for the wall jet with an external stream but no pressure gradient.

A feature of wall jets that has attracted considerable interest is that the point of zero shear stress does not coincide with the point of maximum velocity. In the present experiments the point of zero shear stress lies closer to the wall than the velocity maximum as is also found to be the case for the wall jet in still air (Guitton 1970). Erian & Eskinazi (1964) found that the opposite occurred in a weak wall jet in a positive pressure gradient. The physical explanation of these results appears to be that in wall jets such as that of Erian & Eskinazi where the jet excess velocity is not very large compared with that of the external flow, the turbulence of the boundary-layer region is more vigorous than that in the outer layer and hence diffusion of boundary-layer properties into the outer layer takes place. For stronger wall jets, such as the present one, and for wall jets in still air the opposite occurs.

In the present experiments the value of U_m/U_e was 2·65 (see figure 1 for the meaning of the symbols) and the Reynolds number based on the slot height b and the jet velocity at the slot was $2{\cdot}8 \times 10^4$. The main measurements were made in the region $60 < x/b < 260$, where both the mean velocity and the turbulence profiles were self-preserving.

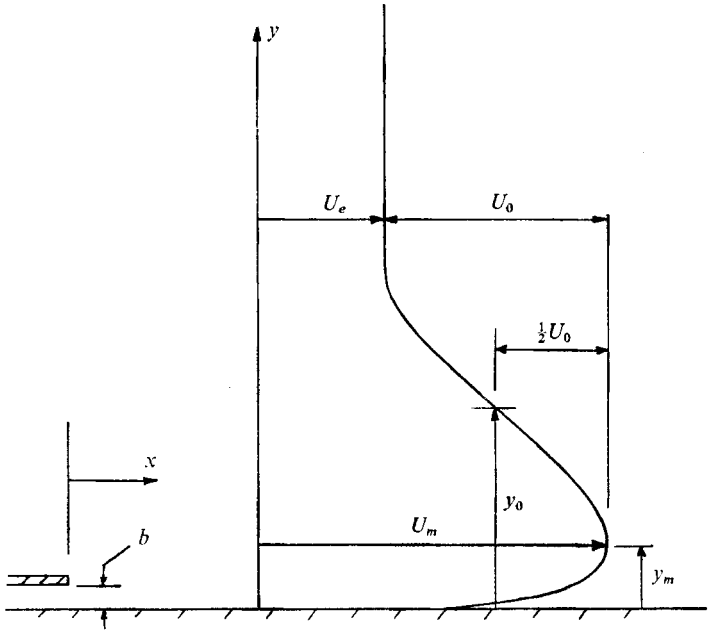

FIGURE 1. Wall jet notation.

2. Theory

2.1. *Conditions for self-preservation from the momentum equation*

Townsend (1956*a*, *b*) investigated in detail the conditions for self-preservation of boundary-layer flows and his approach is followed here. The conditions for self-preservation are obtained by assuming the velocity and turbulence stresses to be given by self-preserving forms and substituting these into the boundary-layer equations. The boundary-layer equations for turbulent flow can be written, neglecting the viscous stress, as

$$\left.\begin{aligned} U\frac{\partial U}{\partial x}+V\frac{\partial U}{\partial y}+\frac{\partial(\overline{u^2}-\overline{v^2})}{\partial x}+\frac{\partial\overline{uv}}{\partial y}=U_e\frac{dU_e}{\partial x}, \\ \partial U/\partial x+\partial V/\partial y=0, \end{aligned}\right\} \tag{1}$$

where U_e is the velocity in the irrotational flow outside the wall jet. The forms for the velocity and turbulence stresses are assumed to be

$$U=U_e+U_0 f(\eta), \quad \overline{uv}=U_0^2 g_{12}(\eta), \quad \overline{u^2}=U_0^2 g_{11}(\eta), \quad \overline{v^2}=U_0^2 g_{22}(\eta), \tag{2}$$

where U_0 is a velocity scale which is a function of x only, $\eta=y/y_0$ and y_0 is a length scale which is also a function of x only. In the present work the scales U_0 and y_0 are defined according to figure 1. Substitution of the above forms into the boundary-layer equations leads (Newman 1967) to

$$\left\{\frac{y_0}{U_0}\frac{\partial U_0}{\partial x}\right\}[f^2+2(g_{11}-g_{22})]+\left\{\frac{y_0}{U_0^2}\frac{d(U_eU_0)}{dx}\right\}f-\left\{\frac{1}{U_0}\frac{dU_e y_0}{dx}\right\}\eta f'-\left\{\frac{1}{U_0}\frac{dU_0 y_0}{dx}\right\}f' \times\int_0^\eta f d\eta-\left\{\frac{dy_0}{dx}\right\}\eta(g_{11}'-g_{22}')+g_{12}'=0, \tag{3}$$

where primes denote differentiation with respect to η. It follows that if f, g_{12}, g_{11} and g_{22} are to be independent of x the terms in the braces must be constants, i.e. dy_0/dx, U_0/U_e and $(y_0/U_0)(dU_0/dx)$ must be constants. Thus

$$y_0 \propto (x+x_0) \tag{4}$$

and

$$U_e \propto (x+x_0)^m, \tag{5}$$

where x_0 is the distance of the hypothetical origin upstream from the slot and the exponent m depends on the ratio U_0/U_e. An equation for the exponent m can be obtained from the boundary conditions and by integration of (3) from $\eta = 0$ to ∞. The necessary boundary conditions are

$$\left.\begin{aligned} &f(\infty) = 0, \quad g_{12}(\infty) = 0, \\ &g_{12}(0) = -u_\tau^2/U_0^2, \end{aligned}\right\} \tag{6}$$

where u_τ is the skin-friction velocity $(\tau_w/\rho)^{\frac{1}{2}}$, τ_w being the shear stress at the wall. It can be seen from (6) that if g_{12} is to be independent of x then u_τ/U_0 must be a constant, i.e. the skin-friction coefficient must be constant. Also, it is known from experiment and dimensional reasoning that near to a wall the velocity scale of the mean flow is u_τ, so that again u_τ/U_0 must be constant for true self-preservation to be possible. Carrying out the integration of (3) from $\eta = 0$ to ∞ and ignoring the normal stress terms the following expression for m is obtained:

$$m = -1/[H(1+1/\beta)+2], \tag{7}$$

where

$$\beta = -\frac{\delta^*}{\gamma^2 U_e}\frac{dU_e}{dx}, \quad \gamma = \frac{u_\tau}{U_e}, \quad \delta^* = \int_0^\infty \left(1-\frac{U}{U_e}\right) dy,$$

$$H = \frac{\delta^*}{\theta}, \quad \theta = \int_0^\infty \frac{U}{U_e}\left(1-\frac{U}{U_e}\right) dy.$$

The parameter β, which is constant for a particular self-preserving flow, is the same as that used by Mellor & Gibson (1966) for boundary layers.

Summarizing, the necessary condition for self-preservation is that $U_e \propto (x+x_0)^m$, where m is given by equation (7), in which it has been assumed that u_τ/U_e is constant. In practice the skin-friction coefficient decreases slightly with increasing x and Mellor & Gibson's analysis of self-preserving boundary layers took some account of this. In the present work it is assumed that the Reynolds number is sufficiently high for the variation of u_τ/U_e to be unimportant.

When the skin friction is zero $|\beta| = \infty$ and so (7) reduces to

$$m = -1/(H+2), \tag{8}$$

which is the expression for m in free turbulent flows (Newman 1967) which are symmetric about $y = 0$. For free jets (8) shows that m ranges from $-\frac{1}{2}$ for a very strong jet ($H = 0$) to $-\frac{1}{3}$ for a very weak jet ($H = 1{\cdot}0$). For wall jets in positive pressure gradients (7) shows that m will be more negative than for a free jet with the same value of H because β is negative.

2.2. *The Reynolds stress and turbulence energy equations*

The Reynolds stress equations contain terms that account for the viscous dissipation of turbulent energy. It is assumed here that the dissipation occurs in a locally isotropic part of the spectrum. It is also assumed that the viscous transport terms may be neglected. With these assumptions and by application of the boundary-layer approximation the Reynolds stress equations for two-dimensional mean flow become

$$\underset{A}{\frac{D(\frac{1}{2}\overline{u^2})}{Dt}} \underset{R}{-\frac{\overline{p}}{\rho}\frac{\partial \overline{u}}{\partial x}} \underbrace{+\overline{u^2}\frac{\partial U}{\partial x}+\overline{uv}\frac{\partial U}{\partial y}}_{P} \underset{DV}{+\frac{\partial(\frac{1}{2}\overline{vu^2})}{\partial y}} \underset{E}{+\frac{\epsilon}{3}} = 0, \tag{9a}$$

$$\underset{A}{\frac{D(\frac{1}{2}\overline{v^2})}{Dt}} \underset{R}{-\frac{\overline{p}}{\rho}\frac{\partial \overline{v}}{\partial y}} \underset{DP}{+\frac{\partial(\overline{pv}/\rho)}{\partial y}} \underset{P}{-\overline{v^2}\frac{\partial U}{\partial x}} \underset{DV}{+\frac{\partial(\frac{1}{2}\overline{v^3})}{\partial y}} \underset{E}{+\frac{\epsilon}{3}} = 0, \tag{9b}$$

$$\underset{A}{\frac{D(\frac{1}{2}\overline{w^2})}{Dt}} \underset{R}{-\frac{\overline{p}}{\rho}\frac{\partial \overline{w}}{\partial z}} \underset{DV}{+\frac{\partial(\frac{1}{2}\overline{vw^2})}{\partial y}} \underset{E}{+\frac{\epsilon}{3}} = 0, \tag{9c}$$

$$\underset{A}{\frac{D\overline{uv}}{Dt}} \underbrace{-\overline{\frac{p}{\rho}\left(\frac{\partial u}{\partial y}+\frac{\partial v}{\partial x}\right)}}_{PS} \underset{P}{+\overline{v^2}\frac{\partial U}{\partial y}} \underset{DV}{+\frac{\partial \overline{uv^2}}{\partial y}} \underset{DP}{+\frac{\partial(\overline{pu}/\rho)}{\partial y}} = 0, \tag{9d}$$

where $D/Dt \equiv U\partial/\partial x + V\partial/\partial y$ and ϵ is the dissipation rate per unit mass. The terms in these equations have been labelled in the following way: $A \equiv$ advection, $R \equiv$ redistribution amongst components of the Reynolds stress, $P \equiv$ production, $DV \equiv$ diffusion by velocity fluctuations, $DP \equiv$ diffusion by pressure fluctuations, $PS \equiv$ pressure–strain correlation and $E \equiv$ dissipation. Addition of the three equations for the normal stresses leads to the equation for the kinetic energy of the turbulence:

$$\underset{A}{\frac{D(\frac{1}{2}\overline{q^2})}{Dt}} \underbrace{+\overline{uv}\frac{\partial U}{\partial y}+(\overline{u^2}-\overline{v^2})\frac{\partial U}{\partial x}}_{P} \underset{DV}{+\frac{\partial(\frac{1}{2}\overline{vq^2})}{\partial y}} \underset{DP}{+\frac{\partial(\overline{pv}/\rho)}{\partial y}} \underset{E}{+\epsilon} = 0, \tag{10}$$

where $q^2 = u^2+v^2+w^2$ and the same labelling applies. It can be shown that the conditions found previously for a self-preserving form of the momentum equation also lead to self-preserving forms of the Reynolds stress and energy equations. For example, in the case of the turbulence energy equation if the following self-preserving forms are assumed

$$\tfrac{1}{2}\overline{q^2} = U_0^2 g(\eta), \quad \overline{pv}/\rho + \tfrac{1}{2}\overline{vq^2} = U_0^3 h(\eta), \quad \epsilon = (U_0^3/y_0)\, e(\eta), \tag{11}$$

then (10) can be written as (Gartshore & Newman 1969)

$$\left\{\frac{y_0 U_e}{U_0^2}\frac{dU_0}{dx}\right\}2g+\left\{\frac{y_0}{U_0}\frac{dU_0}{dx}\right\}2gf-\left\{\frac{1}{U_0}\frac{dy_0 U_e}{dx}\right\}\eta g'-\left\{\frac{1}{U_0}\frac{dy_0 U_0}{dx}\right\}g'\int_0^\eta f\,d\eta+f'g_{12}+h'+e$$
$$+\left\{\frac{y_0}{U_0}\frac{dU_e}{dx}\right\}[g_{11}-g_{22}]+\left\{\frac{y_0}{U_0}\frac{dU_0}{dx}\right\}f(g_{11}-g_{22})-\left\{\frac{dy_0}{dx}\right\}(g_{11}-g_{22})\,\eta f' = 0. \tag{12}$$

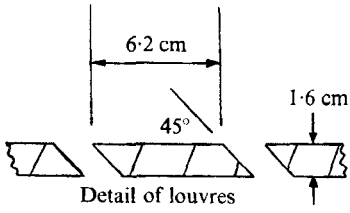

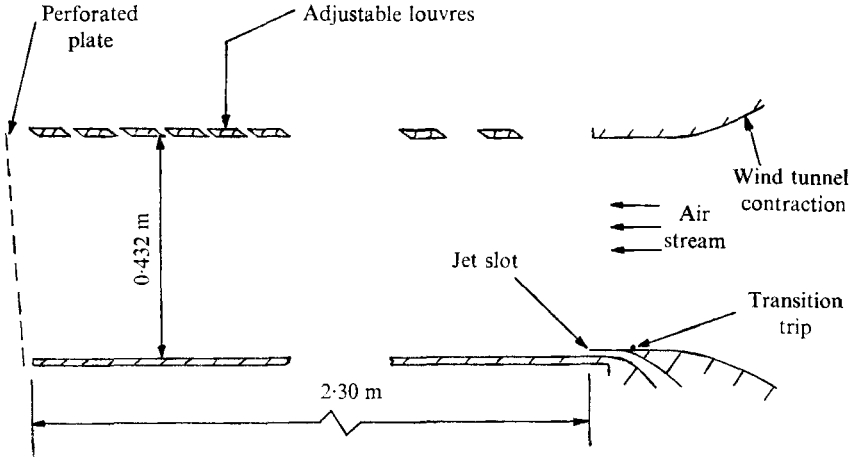

FIGURE 2. Schematic diagram of working section.

It is found that if the conditions for self-preservation derived from the momentum equation are satisfied then the terms in the braces in (12) are automatically constant and thus that (10) is of self-preserving form.

3. Experiments

3.1. *The wind tunnel and jet*

The experiments were carried out in an open-circuit blower-type wind tunnel which has been described by Wygnanski & Gartshore (1963). The tunnel was driven by a single-stage centrifugal fan powered by an 18 kW three-phase constant-speed electric motor and the speed was controlled by variable inlet vanes. The turbulence level was reduced by a honeycomb and three removable screens in the settling chamber upstream of a 6:1 contraction. The screen arrangement used in the experiments is described in a subsequent section. The wall jet emanated from a 6·73 mm high slot with a 3·18 mm thick lip spanning the working section floor at the contraction exit as shown in figure 2. The air for the jet was supplied by a 15 kW centrifugal fan and its temperature could be adjusted to equal that of the wind tunnel air using a water-cooled heat exchanger in the air supply from the fan. The jet velocity was controlled using a throttle between the fan and heat exchanger. Both the wind tunnel and slot air was filtered down to

0·5 μm using American Air-Filter fibreglass filters. The blowing slot was basically the same as that described by Gartshore & Hawaleshka (1964), who took care to eliminate three-dimensional irregularities in the flow. The working section (figure 2) was 0·76 m wide by 0·43 m high and 2·3 m long. The pressure gradient was tailored using adjustable louvres in the roof as shown in figure 2 and a perforated plate at the exit. The floor was Plexiglas except for the final 0·76 m of the working section, which was aluminium and had two streamwise rows of static pressure holes 17·8 cm on either side of the centre-line. In each of the side walls, which consisted of three Plexiglas windows set in wood, there were 6 mm wide vertical slots at 0·3, 1·08 and 1·86 m from the jet slot to allow the side-wall boundary layers to bleed away.

3.2. *Instrumentation*

Pitot-tube and hot-wire traverses were carried out using a traverse gear mounted above the working section. The traverse gear was basically that designed and built by Fekete (1970) for his experiments and consisted of a lead screw driven by synchro receiver which was wired to a transmitter. The transmitter was coupled to a mechanical counter from which the position was read. It was checked for accuracy and found to be accurate to within 0·03 mm over 10 cm. The probe position was 'zeroed' relative to the surface by a reflexion technique to an estimated accuracy of 0·03 mm.

The hot-wire equipment used for measuring turbulence shear and normal stresses consisted of standard DISA normal and inclined wires and a constant-temperature DISA 55D01 control unit, a 55D10 linearizer and a 55D25 auxiliary unit. Root-mean-square voltages were measured using the circuit in a DISA 55D35 unit. The r.m.s. output and mean voltages were fed to an analog scanner and digitized by a VIDAR 521 digital voltmeter; both were part of a central computer facility (GE/PAC 4020) described by Vroomen (1970). Integration times for mean voltages were 10 s, and the r.m.s. circuit was set to a 3 s time constant, the output being sampled ten times at about 1 s intervals and then averaged. For triple and quadruple velocity correlations a DISA X-wire, modified according to the recommendation of Jerome, Guitton & Patel (1971) to avoid thermal wake interference, was used. Additional units identical to those already described were used for the second wire. Two 55A06 correlators were used, one to obtain sums and differences of instantaneous voltages and the other to measure correlation coefficients. Where squaring of instantaneous signals was necessary the squaring circuits of the 55D35 r.m.s. meters were employed. Measurements of the r.m.s. voltages were read directly from the meters and mean voltages on two Hewlett–Packard 2212A V.F. converter/5216 electronic counter combinations. For the measurements of spectra a Brüel & Kjaer 2112 audio frequency spectrometer was employed, having a range from 25 to 40000 Hz. The spectrometer output was read on one of the DISA r.m.s. voltmeters, which had its time constant set to 30 s for the measurements at the low frequency end of the spectrum.

Pressures were measured by a range of Statham unbonded strain gauge transducers, the most sensitive having a range of 0 to 0·07 kN/m^2, and a 48 port

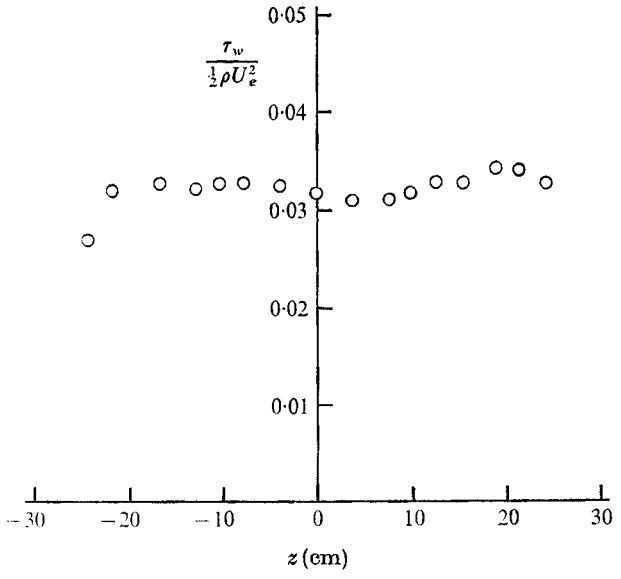

FIGURE 3. Lateral variation of skin friction at $x/b = 200$.

scanivalve facilitated switching amongst the static pressure holes located in the floor of the working section. The transducer outputs were read by the voltmeter in the central computer facility or by a V.F. converter/electronic counter combination. The Pitot tube used for the traverses was cylindrical with an outside diameter of 0·725 mm and had internally sharpened lips to reduce its sensitivity to flow direction. To measure skin friction a 0·254 mm ($\pm 2\%$) thick razor blade was positioned over a static hole and held to the surface by a small piece of adhesive tape at each end. East (1967) has made a detailed calibration of razor blades attached to the surface magnetically and Foster, Irwin & Williams (1971) found that using adhesive tape in the above manner caused no discernible departures from East's calibration. A further check on the calibration is described in a subsequent section.

3.3. *Flow conditions*

Besides being self-preserving the flow also had to be adequately two-dimensional. Before setting the pressure gradient, therefore, a series of trials was carried out to eliminate three-dimensional disturbances from the wind tunnel screens of the kind described by Bradshaw (1963) and Patel (1964), from the slot or from irregular boundary-layer transition upstream of the slot. The final arrangement of the screens consisted of one with $k \simeq 3$ followed by a 3·8 cm deep honeycomb with 6·3 mm cells, the two screens downstream of the honeycomb being removed. Boundary-layer transition was fixed by a 2·3 mm diameter steel rod glued across the floor 8·5 cm upstream of the slot. No special adjustments of the slot were required. After the pressure gradient and wall jet velocity had been set measurements of the lateral variation of skin friction were made using a Preston tube and Patel's (1965) calibration at about 200 slot widths from the slot. The results are shown in figure 3 and the variation can be seen to be less than about $\pm 3\%$ in the central 36 cm of the working section. Since skin friction is a sensitive indicator

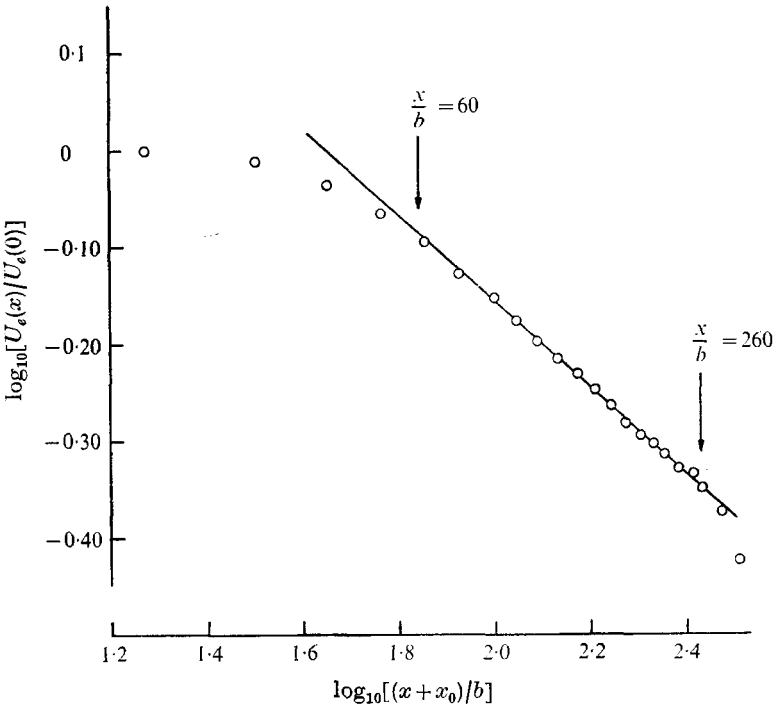

FIGURE 4. Power-law variation of external flow velocity.

of irregularities of a three-dimensional nature the flow was deemed to be adequately two-dimensional. The free-stream turbulence at the exit of the contraction was 0·5% at the speed of the experiments with the above screen arrangement.

The pressure gradient was set by an iterative technique. In order that the exponent m could be accurately estimated in advance a case was chosen that corresponded closely to one of those investigated by Patel & Newman (1961). This enabled H and β to be evaluated from their data and then m could be calculated using (7). The essence of the iterative technique was to assume that the velocity Q_L of the air escaping from between the louvres was given by

$$\tfrac{1}{2}\rho Q_L^2 = \Delta p + K \times \tfrac{1}{2}\rho U_e^2, \tag{13}$$

where Δp is the local pressure difference between the working section interior and the laboratory, and K is an empirical constant. Starting with a guessed value for K of 1 the louvre positions required for a particular value of m could be calculated using (13) and the continuity condition. The value of m actually achieved enabled an improved value of K to be calculated and so on. The final value of K was about 0·7 and incorporates the effect of entrainment into the jet as well as accounting for contraction of the flow between the louvres. The level of Δp was adjusted by blanking off a certain proportion of the perforated plate at the end of the working section (figure 2) with adhesive tape. Further adjustment was possible by altering the angle to the vertical of the perforated plate, which was hinged along its bottom edge. This had the effect of changing the gap between the plate and the last of the slots in the roof of the working section. The final

conditions were $U_0/U_e = 1{\cdot}65$ and $m = -0{\cdot}448$ and the extent of the power-law variation of U_e is shown in figure 4. It was found impossible to obtain a power-law variation for $x/b < 60$, where b is the slot height, and at the downstream end the power-law region was terminated at $x/b \doteq 260$ by an abrupt pressure rise associated with the flow at the end of the working section. The main measurements were carried out in the range $60 < x/b < 260$. The value of the form parameter H was 0·452 ($\pm 0{\cdot}005$) in the self-preserving region and β varied from $-1{\cdot}86$ at $x/b = 82{\cdot}2$ to $-2{\cdot}07$ at $x/b = 248{\cdot}0$, indicating a slight departure from the self-preserving condition due to increasing Reynolds number. It is interesting to note that if skin friction is neglected, i.e. $|\beta| = \infty$, then (7) gives a value for m of $-0{\cdot}408$ for $H = 0{\cdot}452$, which is very different from the value $-0{\cdot}448$ actually required. The significance of a difference of this size can be seen when it is remembered that the total range of m for self-preserving free jets is only $-0{\cdot}50 < m < -0{\cdot}33$.

3.4. *Comments on the data*

The Pitot-tube measurements of mean velocity were corrected for turbulent intensity using the formula

$$\frac{U}{U_{\text{unc}}} = 1 - \frac{1}{2}\left(\frac{\overline{u^2} + \overline{w^2} - \overline{v^2}}{U^2}\right)_{\text{unc}}, \tag{14}$$

where the subscript 'unc' indicates uncorrected quantities. This formula includes the correction for the static pressure variation across the wall jet caused by the transverse turbulent intensity. The measurements were also corrected for displacement using the correction of Macmillan (1956).

The hot-wire data for U, $\overline{uv}$, $\overline{u^2}$, $\overline{v^2}$ and $\overline{w^2}$ were corrected for longitudinal cooling using Champagne, Sleicher & Wehrmann's (1967) correction, which depends on the wire aspect ratio, and for high intensity effects using Guitton's (1970) equations. The correction of Champagne *et al.* was checked by the author before the present experiments were commenced (Irwin 1972). Guitton's corrections include correlations up to fourth order and in the present work assumptions did not have to be made for the third- and fourth-order correlations because all the necessary terms were measured. It transpired that, despite intensities of up to 20 %, the corrections were small, always less than 5 %, owing to near cancellation of many of the terms in the equations. Nevertheless, they were applied since the third- and fourth-order correlations were available. The third- and fourth-order correlations themselves were not, however, corrected for high intensity.

The correlations $\overline{vw^2}$ and $\overline{v^2w^2}$ were measured by aligning the plane of the X-wire parallel to the flow at 45 % to the plane of the x and y axes shown in figure 1. With the assumption that corrections involving odd powers of w were zero, as should be the case for two-dimensional flow, the following relations can be obtained:

$$\overline{(e_1 - e_2)^3} \propto \overline{v^3} + 3\overline{vw^2}, \tag{15a}$$

$$\overline{(e_1 - e_2)^4} \propto \overline{v^4} + 6\overline{v^2w^2} + \overline{w^4}, \tag{15b}$$

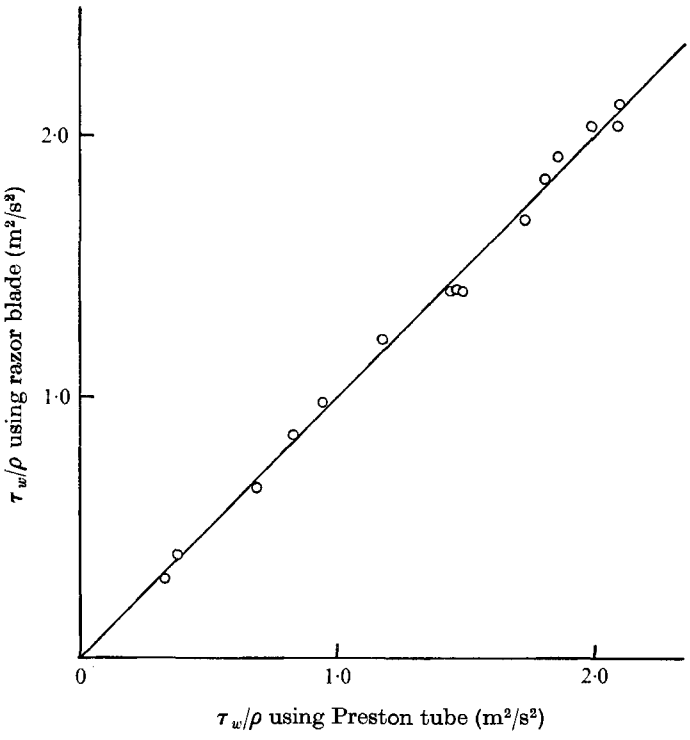

FIGURE 5. Comparison of razor-blade and Preston-tube measurements of skin friction in a zero-pressure-gradient boundary layer. O, measurements; ———, τ_w using razor blade = τ_w using Preston tube.

where e_1 and e_2 are the fluctuating components of the signals from the two wires and A and B are calibration constants. Once $\overline{v^3}$ had been measured with the cross-wire in the x, y plane, $\overline{vw^2}$ could be calculated from (15*a*) (Wygnanski & Fiedler (1969) and Hanjalić & Launder (1972*a*) have also obtained $\overline{vw^2}$ in this way). Similarly, the measurements of $\overline{v^4}$ and $\overline{w^4}$ enabled $\overline{v^2w^2}$ to be calculated from (15*b*). Since the two correlations were obtained in this indirect fashion their accuracy was rather low.

The razor-blade measurements of skin friction were reduced using the calibration formula of East (1967):

$$y^* = -0{\cdot}23 + 0{\cdot}618x^* + 0{\cdot}0165x^{*2}, \tag{16}$$

where $$y^* = \log_{10}[(u_\tau h/\nu)]^2, \quad x^* = \log_{10}[\Delta p h^2/\rho\nu^2],$$

Δp is the difference between the pressure measured at the static hole with the razor blade in position and with it removed and h is the height of the blade cutting edge above the surface. Since the blades were laid flush with the surface h was assumed to be half the blade thickness, i.e. 0·127 mm. Care was taken to clean the surface thoroughly before attaching each blade because small particles of dust would have introduced large errors in h. The technique was checked by comparing razor-blade measurements with those of a 1·577 mm diameter Preston

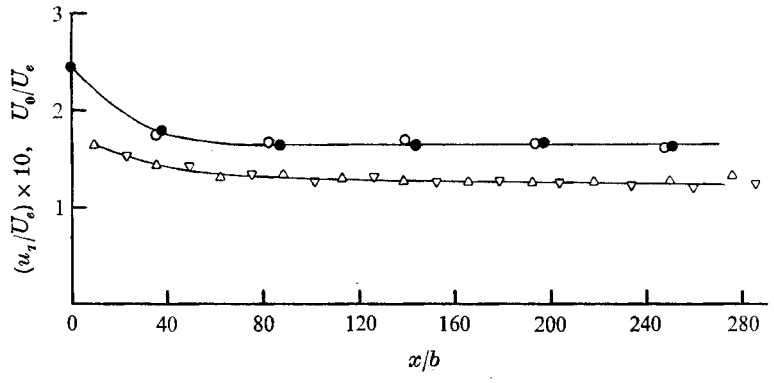

FIGURE 6. Variation of U_0/U_e and u_τ/U_e. U_0/U_e: ●, Pitot tube; ○, hot wire. △, ▽, razor-blade measurements of u_τ/U_e at 17·8 cm either side of the centre-line of the working section.

tube, using the calibration of Patel (1965), in a zero-pressure-gradient boundary layer and the results, which are shown in figure 5, are in good agreement.

The zero-pressure-gradient boundary layer was produced by putting a solid roof into the working section and raising the floor so that it lay flush with the upper surface of the slot lip. The different levels of skin friction were obtained by varying the wind speed in the range 6–40 m/s and using different x stations. The Preston-tube and razor-blade measurements were made at identical positions. In the wall jet experiments the value of $u_\tau h/\nu$ for the blades was less than 11 for $x/b > 140$, was 14·6 at $x/b = 82{\cdot}2$ and was 21·0 at $x/b = 35{\cdot}7$. Thus the measurements did not extend beyond the 'buffer' region, and over most of the self-preserving section of the flow they were within the viscous sublayer and should therefore have been insensitive to possible changes in the constants of the logarithmic law of the wall.

4. Experimental results

4.1. *Mean flow data*

The variation of U_0/U_e and u_τ/U_e is shown in figure 6. The value of U_0/U_e was effectively constant and equal to 1·65 for $x/b > 60$ and u_τ/U_e, obtained from razor-blade measurements at the static hole positions on either side of the working section centre-line, decreased by about 5 % over the range $60 < x/b < 260$. In figure 7 the present skin-friction results and those of Patel (1962) for the same experimental conditions are compared with empirical formulae for wall jets in zero pressure gradients. The formula which has most experimental support is that for the wall jet in still air. Guitton (1970) critically examined the available skin-friction data for this case as well as carrying out careful measurements of his own and concluded that the data are reasonably well fitted by

$$C_f = 0{\cdot}0315(U_m y_m/\nu)^{-0{\cdot}182}, \tag{17a}$$

where $C_f = \tau_w/\frac{1}{2}\rho U_m^2$. This formula had originally been proposed for the still-air case by Bradshaw & Gee (1962), but on the basis of less experimental evidence.

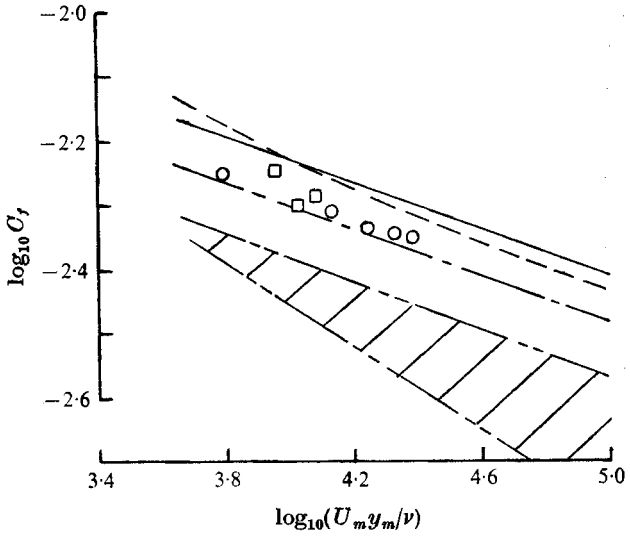

FIGURE 7. Comparison of skin friction with empirical laws for wall jets in a zero pressure gradient. ○, present data; □, data of Patel (1962); ——, Guitton (1970), $U_m/U_e = \infty$; —·—, Bradshaw & Gee (1962), equation (17*b*), $1 < U_m/U_e < 2$; ////, Kruka & Eskinazi (1964), $1{\cdot}2 < U_m/U_e < 14$; – – – –, McGahan (1965), $1{\cdot}05 < U_m/U_e < \infty$.

Although (17*a*) agrees quantitatively with the available still-air data the precise dependence of C_f on Reynolds number is still rather uncertain because of the small Reynolds-number range of the experiments, roughly $3 \times 10^3 < U_m y_m/\nu < 3 \times 10^4$. For the wall jet with an external stream in zero pressure gradient Bradshaw & Gee (1962) and Kruka & Eskinazi (1964) have proposed formulae of the same form as (17*a*) but with different constants, the constants of Kruka & Eskinazi being dependent on the ratio of the jet velocity to the free-stream velocity. McGahan (1965) proposed a different formula based on assumptions about the velocity profile, without recourse to measurements of skin friction. It can be seen in figure 7 that the three proposals for the wall jet with an external stream do not agree with each other but that Bradshaw & Gee's is close to the present and Patel's data. McGahan's formula appears to be slightly less accurate. The formulae of Kruka & Eskinazi fail to approach the fairly well established results for the wall jet in still air as U_m/U_e becomes large, the value of C_f being far too low, which implies that the experimental data on which they were based are inaccurate. Those of Bradshaw & Gee may have suffered from a lack of two-dimensionality but it seems likely that this was not too serious because their results for the still-air wall jet, obtained from the same apparatus, agree well with subsequent more definite data (Guitton 1970). On balance then it seems that the formula of Bradshaw & Gee (1962),

$$C_f = 0{\cdot}026\,(U_m y_m/\nu)^{-0{\cdot}18}, \tag{17b}$$

is the most reliable at present for the wall jet with an external stream in zero pressure gradient for low values of U_m/U_e. If (17*b*) does accurately represent the zero-pressure-gradient case then the closeness of the present and Patel's

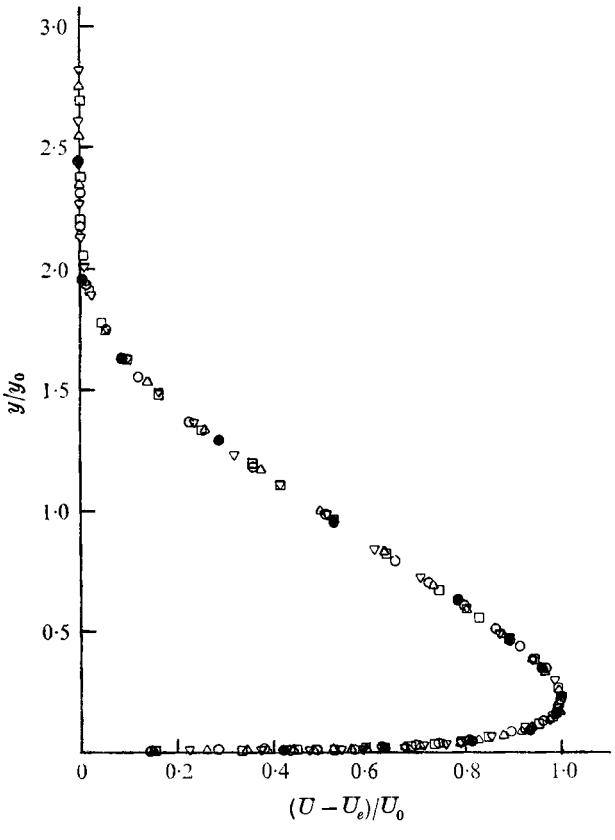

FIGURE 8. Mean velocity profiles. Hot-wire data: ○, $x/b = 82{\cdot}2$; □, $x/b = 139{\cdot}5$; ▽, $x/b = 194{\cdot}0$; △, $x/b = 248{\cdot}0$. ●, Pitot-tube data, $x/b = 251{\cdot}0$.

results to it in figure 7 would suggest that the pressure gradient has little influence on the skin friction. However, this must remain a tentative conclusion until the value of the skin friction in the zero-pressure-gradient case is more firmly established.

Mean velocity profiles, which were measured using hot wires at four stations in the region $60 < x/b < 260$, are shown in figure 8 and it can be seen that the scales y_0 and U_0 produce a good collapse of the data. A few of the Pitot-tube measurements from one station are included to show the level of agreement with the hot-wire data, which can be seen to be good. In figure 9 the inner layer is given in more detail and shows a trend towards higher values of $(U-U_e)/U_0$ at a given η as x increases. This can be attributed to the gradual decrease in u_τ/U_e. A conventional semi-logarithmic plot of the hot-wire results for mean velocity in the wall region is shown in figure 10. The skin-friction velocity was that read from a mean curve through the razor-blade measurements. From the results of Wills (1963) it was deduced that the effect of heat loss from the wire to the wall was negligible within the logarithmic region. The measurements are compared with the logarithmic law of the wall, the values of the constants being those recommended by Patel (1965):

$$u_+ = 5{\cdot}5 \log_{10} y_+ + 5{\cdot}45, \tag{18a}$$

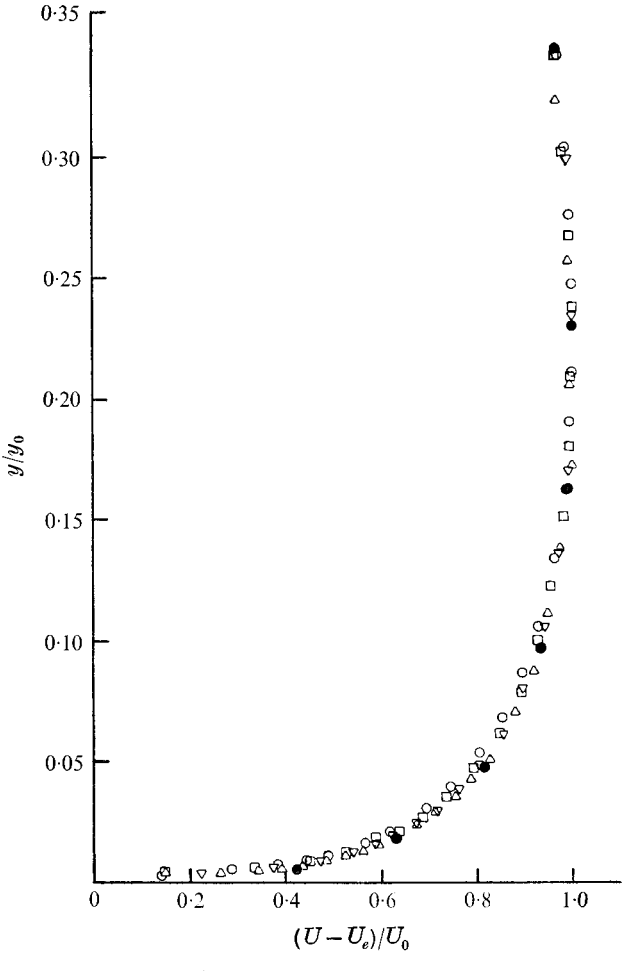

FIGURE 9. Mean velocity profiles in inner region. Notation as in figure 8.

where $u_+ = U/u_\tau$ and $y_+ = u_\tau y/\nu$. The logarithmic law can be derived by similarity arguments when the shear stress is constant and equal to its value at the wall (Rotta 1962). Townsend (1961) derived a more general expression, which is also shown in figure 10, from the turbulence energy equation assuming a linear variation of the shear stress $\tau = \tau_w + \alpha y$, the constant α being negative in the present case. With Patel's constants it can be written as

$$\frac{U}{u_\tau} = 5{\cdot}5 \log_{10}\left[y_+\left\{\frac{4}{T}\frac{(1+T)^{\frac{1}{2}}-T}{(1+T)^{\frac{1}{2}}+T}\right\}\right] + 5{\cdot}45 + 4{\cdot}78\,(1-B\,\mathrm{sgn}\,\alpha)\,((1+T)^{\frac{1}{2}}-1), \quad (18b)$$

where $T = y_+ \partial\tau_+/\partial y_+$, $\tau_+ = \tau/\tau_w$ and B is a diffusion constant. Equation (18*b*) is valid provided that structural similarity of the turbulence exists, advection of turbulence energy is negligible and that at the inner edge of the turbulent flow, i.e. at $y_+ \simeq 20$, $|T| \ll 1$. The last condition was fairly well satisfied in the present experiments, $\partial\tau_+/\partial y_+$ varying from approximately $-0{\cdot}0020$ to $-0{\cdot}0013$ in the

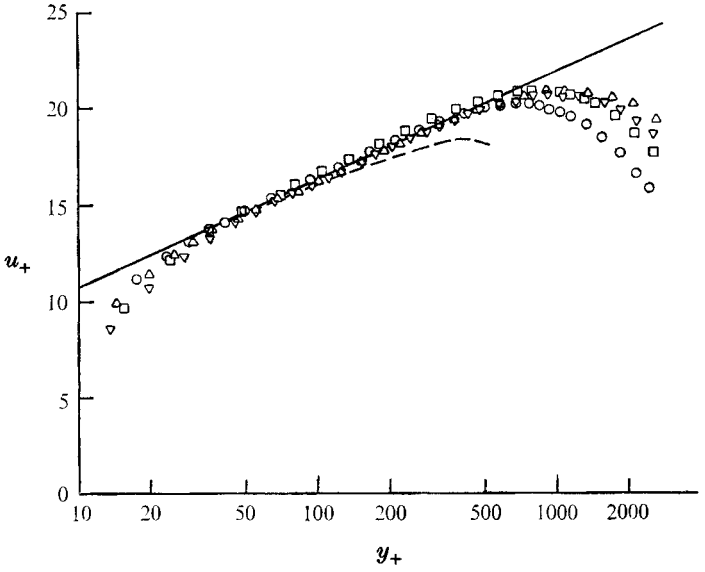

FIGURE 10. Semi-logarithmic plot of mean velocity in the wall region. Hot-wire data: ○, $x/b = 82{\cdot}2$, $(U_m y_m/\nu) \times 10^{-4} = 1{\cdot}37$; □, $x/b = 139{\cdot}5$, $(U_m y_m/\nu) \times 10^{-4} = 1{\cdot}77$; ▽, $x/b = 194{\cdot}0$, $U_m(y_m/\nu) \times 10^{-4} = 2{\cdot}15$; △, $x/b = 248{\cdot}0$, $(U_m y_m/\nu) \times 10^{-4} = 2{\cdot}42$. ——. law of the wall according to Patel (1965); – – –, equation (18*b*).

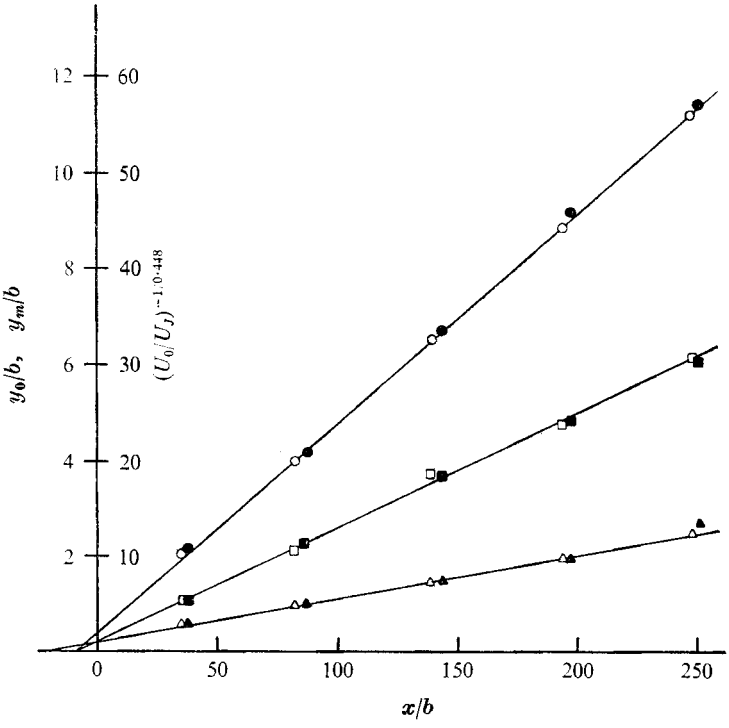

FIGURE 11. Variation of length and velocity scales. Open symbols, hot-wire data; solid symbols, Pitot-tube data. ○, y_0/b; △, y_m/b; □, $(U_0/U_J)^{-0/0{\cdot}448}$.

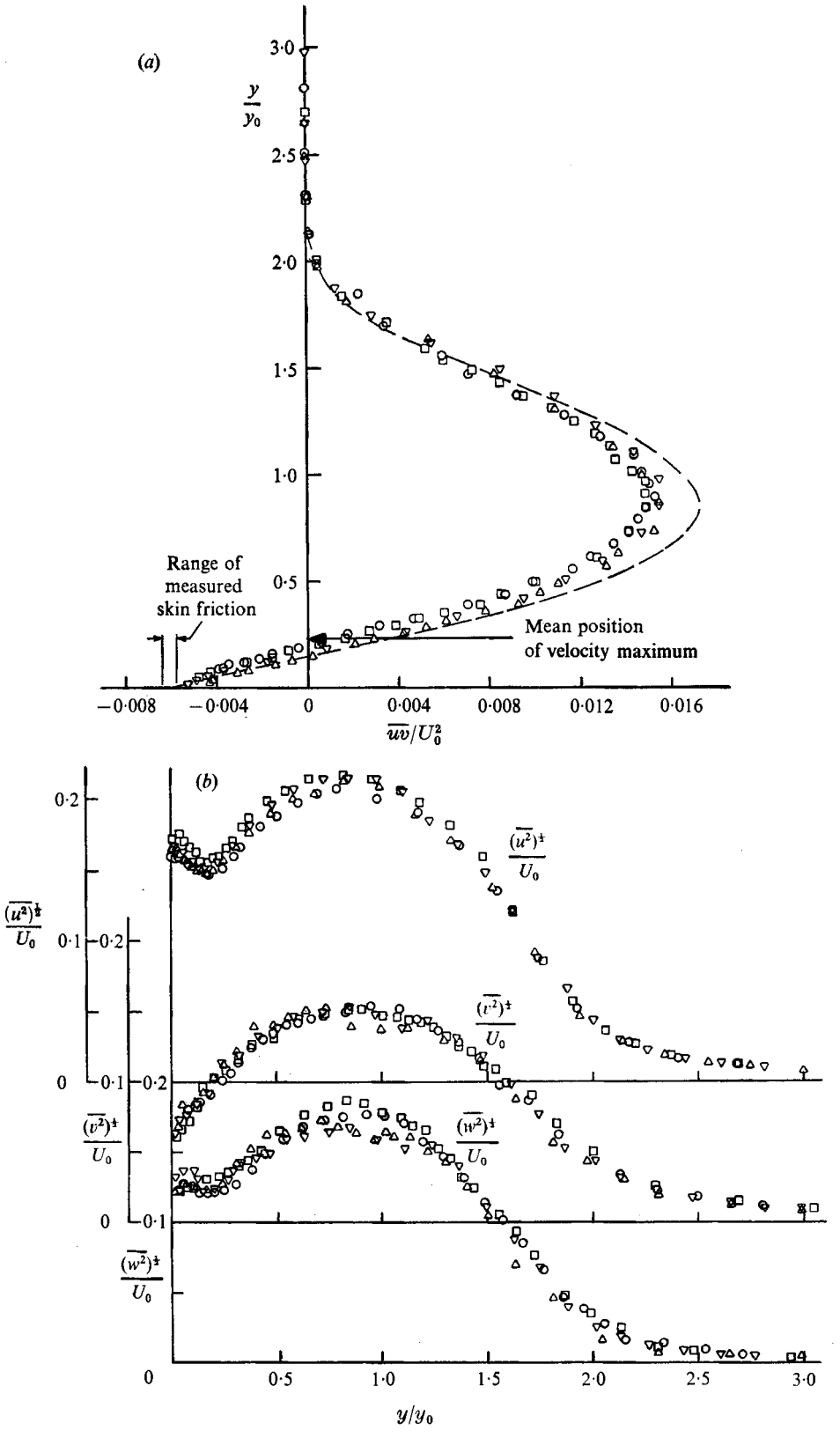

FIGURE 12. Distribution of (*a*) $\overline{uv}$ and (*b*) turbulence intensities across wall jet. Hot-wire measurements: ○, $x/b = 82{\cdot}2$; □, $x/b = 139{\cdot}5$; ▽, $x/b = 194{\cdot}0$; △, $x/b = 248{\cdot}0$. – – –, $\overline{uv}$ calculated from the mean momentum equation.

self-preserving region. A mean value for $\partial\tau_+/\partial y_+$ of $-0{\cdot}0017$ was chosen and Townsend's value of 0·2 for B was used in comparing (18*b*) with the data in figure 10. It can be seen that for y_+ less than about 150 equations (18*a*) and (18*b*) are not very different and agree well with the data. For higher values of y_+ equation (18*b*) is significantly different from the data indicating that the assumptions of structural similarity and negligible advection, which are implicit in both equations (18), are no longer valid. Equation (18*a*) continues to agree with the measurements for values of y_+ as high as 500 but this is considered to be fortuitous. These results are consistent with the more recent measurements for the wall jet in still air at similar Reynolds numbers, $U_m y_m/\nu \doteq 10^4$, which show that the usual logarithmic law (18*a*) applies but over the rather restricted range of approximately $30 < y_+ < 150$ (Guitton 1970).

The measured values of y_0 and y_m are shown in figure 11 together with $(U_0/U_J)^{-1/0{\cdot}448}$, U_J being the jet velocity at the slot. The Pitot-tube and hot-wire results are in good agreement. The virtual origins for y_0 and U_0 were very close to each other but that for y_m was slightly further upstream. The rate of growth dy_0/dx was 0·0436, which is almost identical to that found by Patel & Newman (1961) for the same U_0/U_e. The Reynolds number $U_m y_m/\nu$ varied from $1{\cdot}3 \times 10^4$ to $2{\cdot}5 \times 10^4$ over the self-preserving region.

4.2. *Turbulence shear stress and intensities*

The shear stress and intensities measured at four stations are shown in figures 12 (*a*) and (*b*). The data were initially made non-dimensional using U_e as a velocity scale and the scales in the figures have been adjusted using the mean value of U_0/U_e in order to express the results in terms of U_0. The measurements show that the turbulence was in a closely self-preserving state except for a slight tendency for the point of zero shear stress to occur at lower values of η as x increased. The latter effect is another manifestation of the weak Reynolds-number dependence of the inner layer. The range of measured skin friction in the region of the traverses is shown in figure 12 (*a*) and it can be seen to be in good agreement with the $\overline{uv}$ data. The shear stress obtained from the momentum equation, including the normal stress terms, and the measured velocity profiles is also shown in figure 12 (*a*). The agreement at the wall is very good but there is a discrepancy of about 13 % at the point of maximum $\overline{uv}$. It may be noted that neglect of the normal stress terms would have *reduced* the latter to about 7 %. Considering the severity of the adverse pressure gradient this order of discrepancy is considered to be quite good.

The main features of $\overline{u^2}$, $\overline{v^2}$ and $\overline{w^2}$ in figure 12 (*b*) are that they all reach their maximum values at about the same position as the maximum shear stress. $\overline{u^2}$ exhibits a minimum near the position of zero shear stress, $\overline{w^2}$ is almost constant in the inner layer and $\overline{v^2}$ decreases monotonically from its maximum value to zero at the wall. Over most of the wall jet $\overline{u^2}$ is the largest of the three intensities but, for $\eta > 2{\cdot}0$, $\overline{v^2}$ becomes slightly larger. The maximum value of $(\overline{u^2})^{\frac{1}{2}}/U$ was about 20 % and this occurred at $\eta \doteq 1{\cdot}3$.

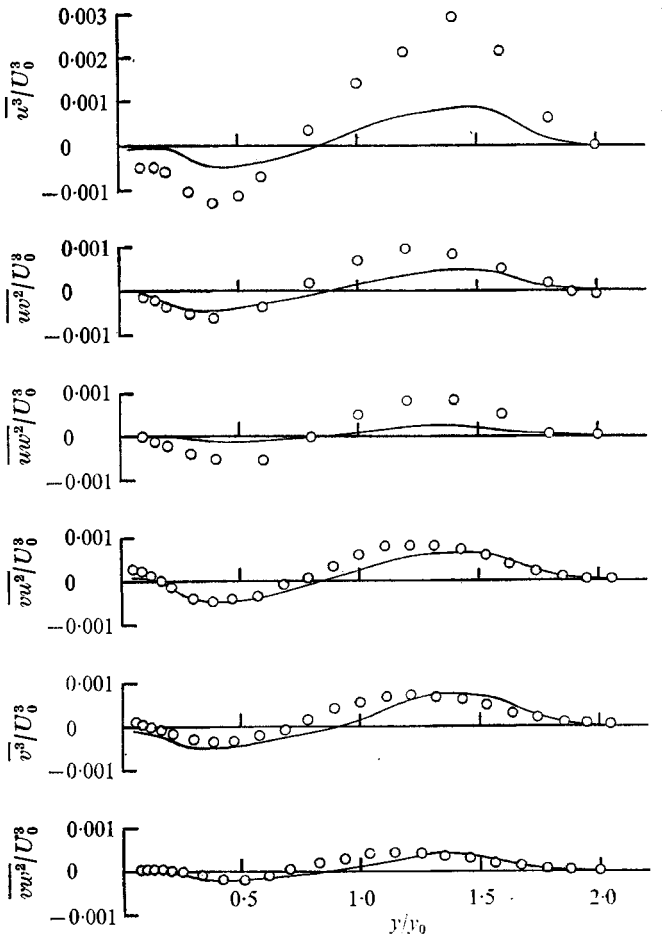

FIGURE 13. Distribution of triple velocity correlation across wall jet. ○, measured values, $x/b = 194{\cdot}0$; ——, model of Hanjalić & Launder (1972*b*); equations (23).

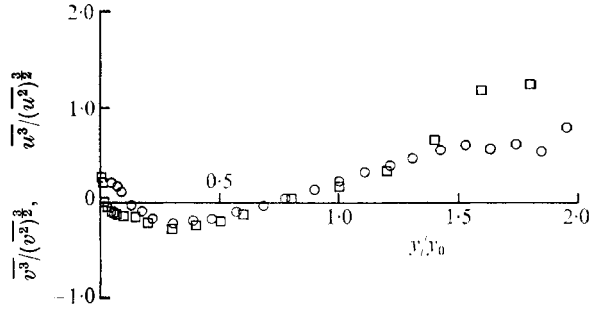

FIGURE 14. Skewness factors. □, $\overline{u^3}/(\overline{u^2})^{\frac{3}{2}}$; ○, $\overline{v^3}/(\overline{v^2})^{\frac{3}{2}}$. $x/b = 194{\cdot}0$.

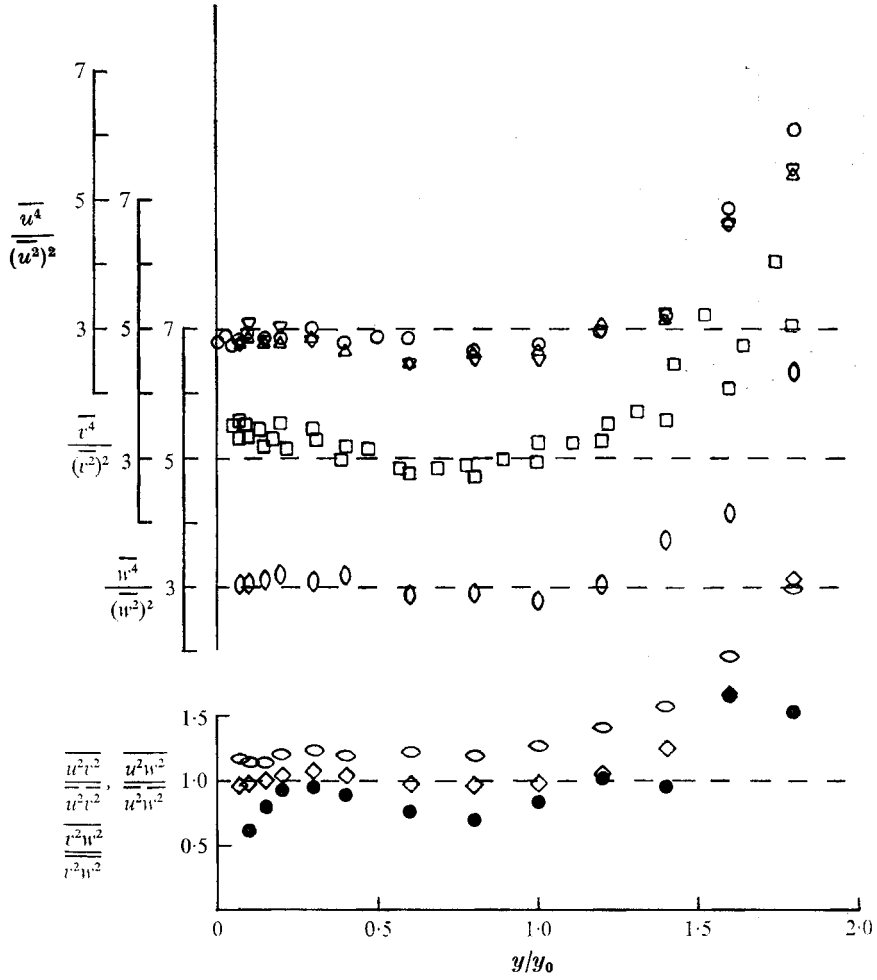

FIGURE 15. Fourth-order velocity correlations. $\overline{u^4}/(\overline{u^2})^2$: ○, normal wire; △, X-wire in horizontal plane; ▽, X-wire in vertical plane. □, $\overline{v^4}/(\overline{v^2})^2$; ◊, $\overline{w^4}/(\overline{w^2})^2$; ⬭, $\overline{u^2v^2}/\overline{u^2}\,\overline{v^2}$; ◇, $\overline{u^2w^2}/\overline{u^2}\,\overline{w^2}$; ●, $\overline{v^2w^2}/\overline{v^2}\,\overline{w^2}$. $x/b = 194$.

4.3. *Higher order correlations*

The triple velocity correlations are shown in figure (13). The most interesting of these are $\overline{vu^2}$, $\overline{v^2}$, $\overline{vw^2}$ and $\overline{uv^2}$ since they occur in the diffusion terms in the boundary-layer form of the Reynolds stress equations (9). The two others, $\overline{u^3}$ and $\overline{uw^2}$, disappear from the equations when the boundary-layer approximation is applied. All the triple velocity correlations pass through zero in the range $0{\cdot}7 < \eta < 0{\cdot}8$, which is slightly nearer to the wall than the position of maximum $\overline{uv}$. The skewness factors of u and v are shown in figure (14). They both vary in a similar manner except in the inner layer and in the intermittent part of the outer layer. For $\eta < 0{\cdot}8$ the skewness factors resemble very much those of Hanjalić & Launder (1972*a*) in their asymmetric channel flow, the skewness of u tending to be more negative than that of v and the two being of opposite sign to each other over a large proportion of the inner layer $0{\cdot}02 < y/y_0 < 0{\cdot}12$. The large values at the

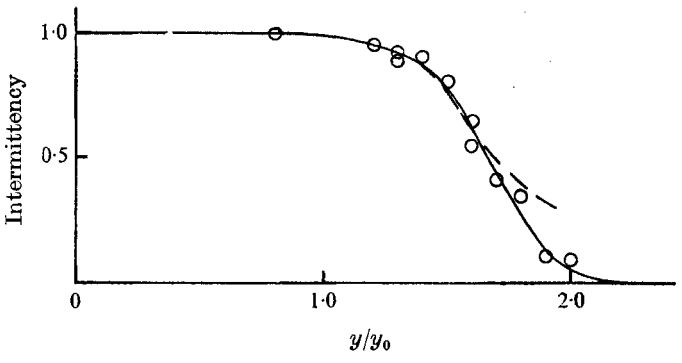

FIGURE 16. Intermittency measurements. —○—, from mirror galvanometer traces; ---, from flatness factor of u. $x/b = 194{\cdot}0$

edge of the flow are attributed to the intermittent nature of the flow there. The level of accuracy for the triple correlations is estimated to be about 15 % of the peak values.

In figure 15 some of the fourth-order correlations which were measured for the purpose of making high intensity corrections are shown. The flatness factors of u, v and w are close to the Gaussian value of 3·0 in the fully turbulent region, which extends from the wall to roughly $\eta = 1{\cdot}2$, but rise to higher values in the intermittent zone. The value of $\overline{u^2w^2}/\overline{u^2}\,\overline{w^2}$ is close to unity in the fully turbulent region whereas $\overline{u^2v^2}/\overline{u^2}\,\overline{v^2}$ is nearer to 1·2. This indicates that the fluctuating component of u^2 is almost independent of that of w^2 but is positively correlated to a certain extent with that of v^2 as might be expected because of the mean velocity gradient. The measurements of $\overline{v^2w^2}/\overline{v^2}\,\overline{w^2}$, which are less reliable than the other fourth-order correlations because of the indirect method by which they were obtained (see § 3.4), lie below unity in the fully turbulent region except near to the velocity maximum, indicating some negative correlation between the fluctuating components of v^2 and w^2.

4.4. *Intermittency*

The intermittency distribution was measured using a mirror-galvanometer chart recorder with a frequency response which was 3 db down at 3 kHz. The $\partial u/\partial t$ signal obtained from the differentiation circuit of one of the correlators was recorded. The results, which were obtained by visual observation of the records, are shown in figure 16. Gartshore (1965) measured the intermittency of several self-preserving wall jets, the two closest to the present case having U_0/U_e equal to 1·92 and 0·91. The points where the measured intermittency was $\frac{1}{2}$ for these two cases were at $\eta = 1{\cdot}56$ and 1·43 respectively which gives an interpolated value of $\eta = 1{\cdot}53$ for the present case. This compares with $\eta = 1{\cdot}66$ measured in the present tests. The difference between these two results illustrates the degree of subjectivity which inevitably enters into the definition of intermittency, however it is measured.

The ratio $[\overline{u^4}/(\overline{u^2})^2]_{\eta=0{\cdot}8}/[\overline{u^4}/(\overline{u^2})^2]_{\eta>0{\cdot}8}$ is also plotted in figure 16 and tends to take higher values than the intermittency for η greater than about 1·6. A similar

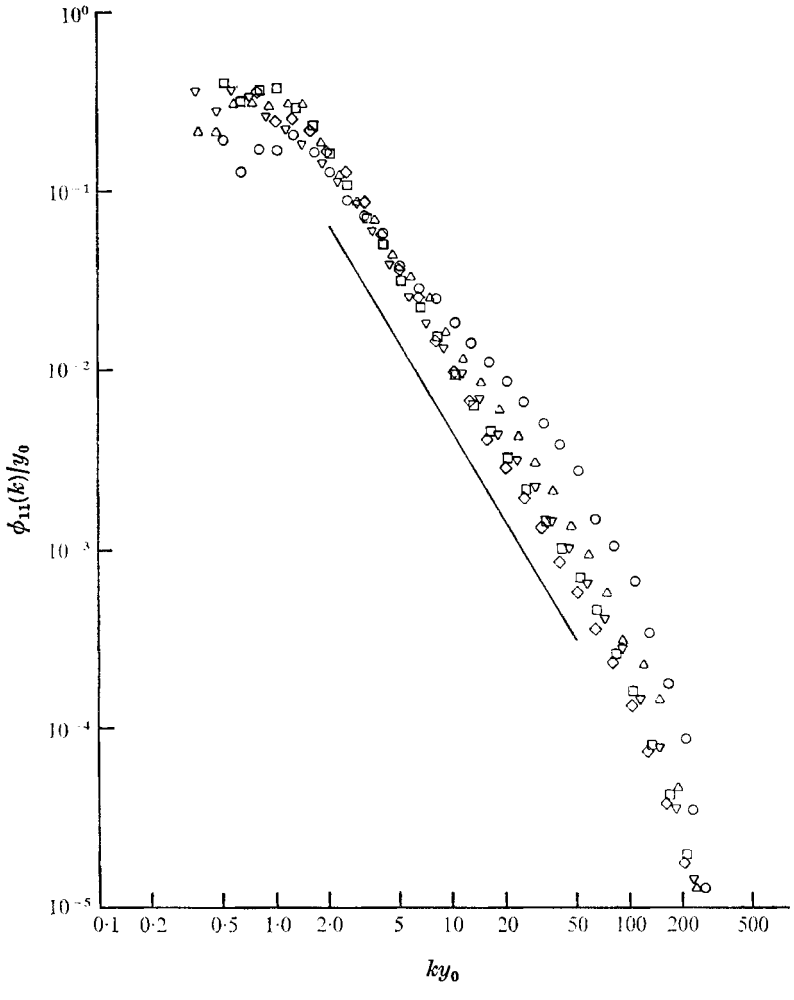

FIGURE 17. Spectra of $\overline{u^2}$ at different positions across wall jet. ○, $y/y_0 = 0{\cdot}0084$; △, $y/y_0 = 0{\cdot}084$; ▽, $y/y_0 = 0{\cdot}24$; □, $y/y_0 = 1{\cdot}0$; ◇, $y/y_0 = 1{\cdot}6$; ——, slope of $-\frac{5}{3}$ law. $x/b = 194{\cdot}0$.

effect was observed in the measurements of Wygananski & Fiedler (1969), where it was attributed to the velocity fluctuations in the irrotational flow.

4.5. *Spectra and dissipation measurements*

The spectrum function $\phi_{ij}(k)$ of $\overline{u_i u_j}$ is defined such that

$$\int_0^\infty \phi_{ij}(k)\,dk = 1, \tag{19}$$

where $k = 2\pi f/U$ and f is the frequency in Hz. Only ϕ_{11} was measured and this was done at a number of points across the wall jet at $x/b = 194$. A representative selection of the results is shown in figure 17. In the outer layer a significant range of $-\frac{5}{3}$ law existed and, following Bradshaw (1967), it was used to obtain the dissipation rate. The same method was used in the inner layer, despite the lack of

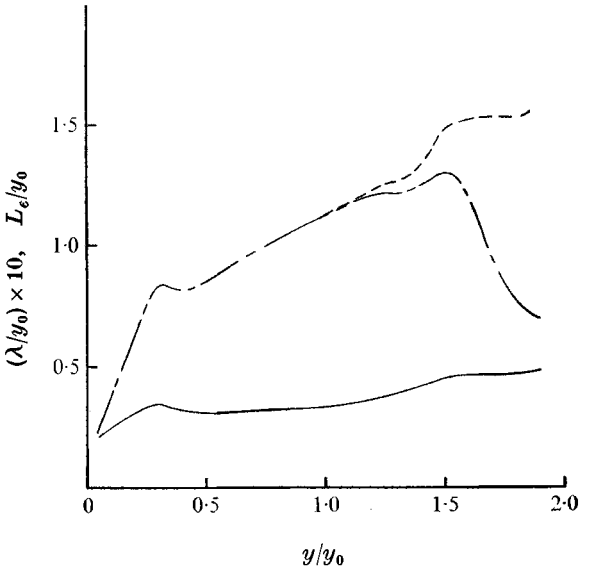

FIGURE 18. Microscale and dissipation length scale. ——, λ/y_0; —·—, L_ϵ/y_0; – – –, L_ϵ/y_0 within turbulent fluid. $x/b = 194{\cdot}0$.

a clear $-\frac{5}{3}$ region, by drawing a tangent of the appropriate slope to the data. For this reason the measured dissipation was not very reliable for $\eta < 0{\cdot}15$. The $-\frac{5}{3}$ law can be expressed as

$$\overline{u^2}\phi_{11}(k) = K\epsilon^{\frac{2}{3}}k^{-\frac{5}{3}}, \tag{20}$$

where K is a constant. There is some variation in the reported values of K, which is partly due to the choice of convection velocity for calculating the wavenumber from frequency. Fortunately there is an indirect check on the calculated dissipation. The diffusion term in the energy equation, when obtained by difference from the other three terms, should integrate to zero across the flow. The value of K was therefore adjusted until this occurred and was found to be 0·45. This is in quite good agreement with Bradshaw & Ferriss (1965), Grant, Stewart & Moilliet (1962) and with Pond, Stewart & Burling (1963). The value of the turbulence Reynolds number $(\overline{u^2})^{\frac{1}{2}}\lambda/\nu$, where $\lambda^2 = 15\nu\ \overline{u^2}/\epsilon$, was about 400 at $\eta = 1{\cdot}0$. This satisfies the condition of Bradshaw (1967) that $(\overline{u^2})^{\frac{1}{2}}\lambda/\nu$ be greater than 100 for an inertial subrange to exist.

An attempt was also made to measure the dissipation rate using the assumption of local isotropy

$$\epsilon = 15\nu\overline{(\partial u/\partial x)^2}. \tag{21}$$

Invoking Taylor's hypothesis, $\overline{(\partial u/\partial x)^2}$ was approximated by $U^{-2}\overline{(\partial u/\partial t)^2}$ and $\partial u/\partial t$ was obtained from one of the DISA correlators. It was found however that a correction of order 100 % was required for the effect of finite wire length. (In the $-\frac{5}{3}$ law range of the measurements there was no significant effect of finite wire length, y_0/l_{wire} being 60.) This, combined with the possible inaccuracy of Taylor's hypothesis, makes these measurements of doubtful validity and they

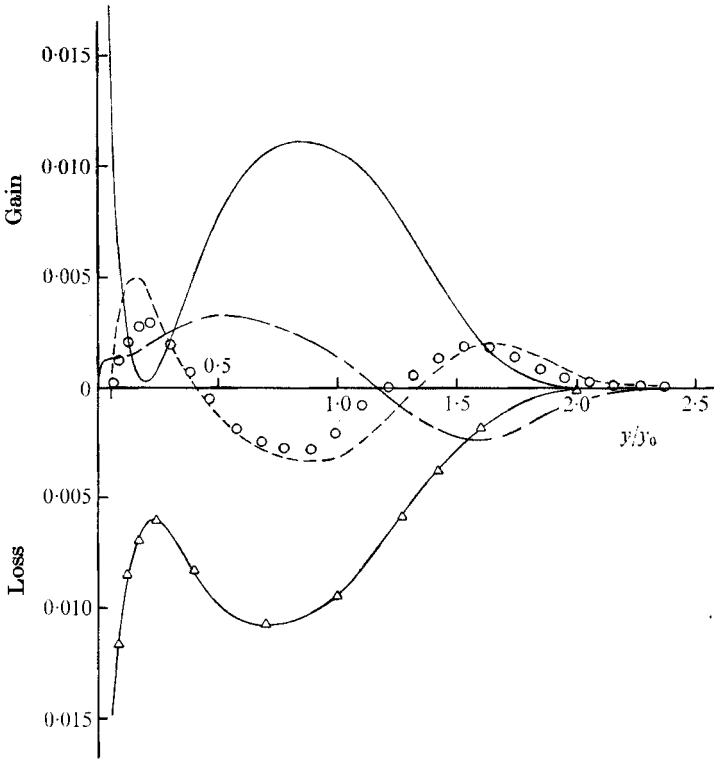

FIGURE 19. Turbulence energy balance. —·—, advection; ——, production; – – –, total diffusion (by difference); ○, velocity diffusion (measured); –△–, dissipation. $x/b = 194{\cdot}0$.

are not presented here. However, it is worth mentioning that the dissipation rate measured in this way agreed to within 25 % with the $-\frac{5}{3}$ law results when the finite wire length correction of Wyngaard (1969) was applied.

The microscale $\lambda = (15\nu\overline{u^2}/\epsilon)^{\frac{1}{2}}$ and the dissipation length $L_\epsilon = (\frac{1}{2}\overline{q^2})^{\frac{3}{2}}/\epsilon$ are shown in figure 18. Also shown is the value of L_ϵ within the turbulent fluid, which was calculated using the measured intermittency assuming $\overline{q^2}$ to be negligible in the irrotational fluid.

4.6. *Energy balance*

In figure 19 the various terms in the energy equation (10) are shown. The production and advection terms were obtained from mean curves drawn through the data from the four traverse positions in the self-preserving region and a three-point formula was used for differentiation. The production term, it may be noticed, does not change sign at the velocity maximum $\eta \simeq 0{\cdot}22$ owing to the contribution of the normal stress term $(\overline{u^2}-\overline{v^2})\,\partial U/\partial x$, which is of the same order as $\overline{uv}\,\partial U/\partial y$ near to the velocity maximum. The measurements of Tailland & Mathieu (1967) indicate that this is also true for the wall jet in still air but for some wall jets with an external flow in a zero pressure gradient there is evidence (Erian & Eskinazi 1964; Kacker & Whitelaw 1969) that the total production term does change sign.

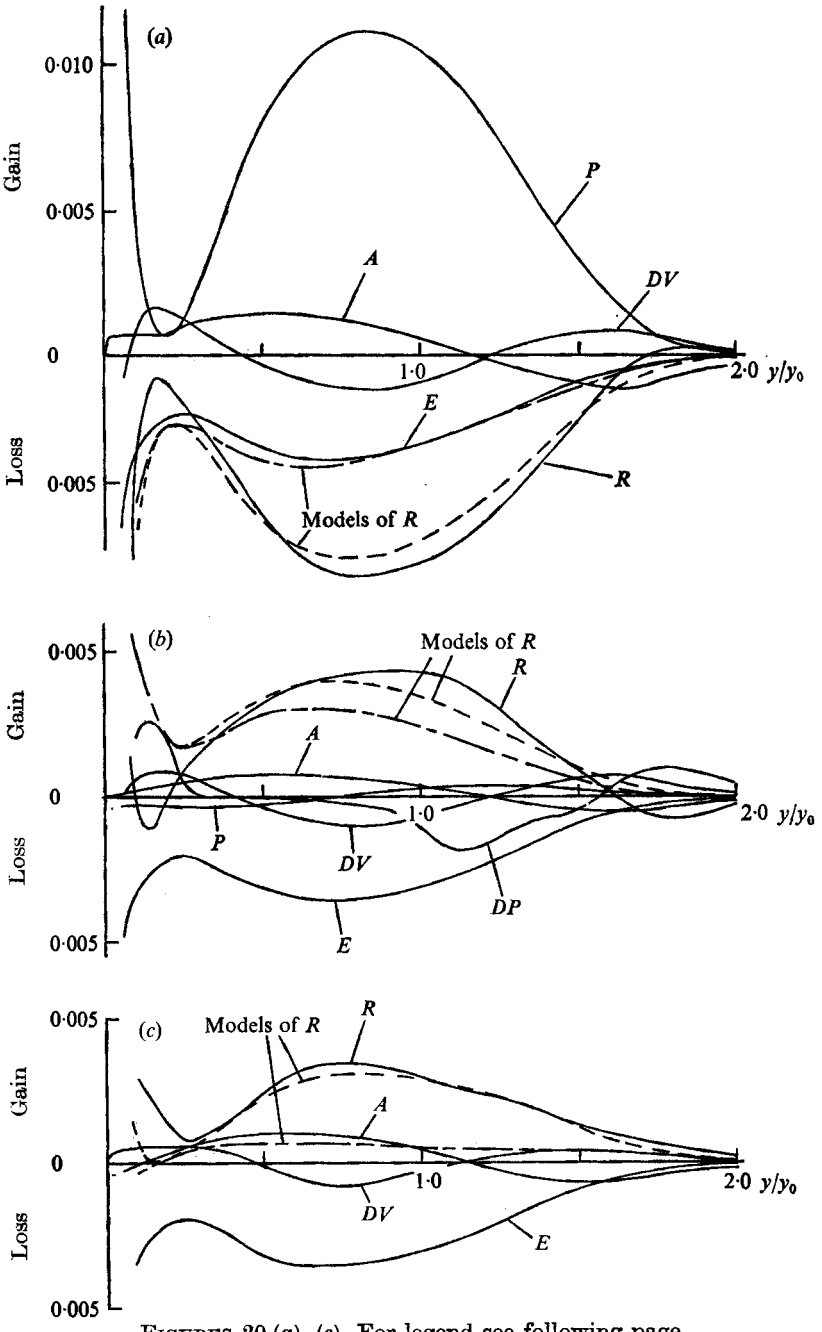

FIGURES 20 (*a*)–(*c*). For legend see following page.

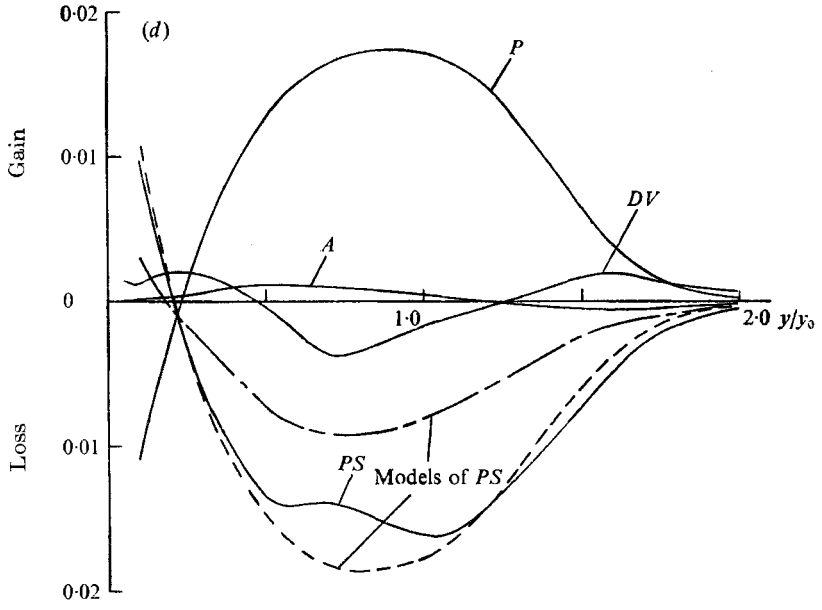

FIGURE 20. Balance of terms in the Reynolds stress equations. A, advection; R, redistribution; P, production; DV, 'velocity' diffusion; DP, 'pressure' diffusion; PS, pressure–strain correlation; E, dissipation. Model of Hanjalić & Launder (1972*b*): ———, without mean rate-of-strain term; – – – –, with mean rate-of-strain term. (*a*) Contribution to $\overline{u^2}$ equation. (*b*) Contribution to $\overline{v^2}$ equation. (*c*) Contribution to $\overline{w^2}$ equation. (*d*) Contribution to $\overline{uv}$ equation.

A check was made to see if the neglect of the slight changes in mean velocity and shear stress profiles due to Reynolds-number effects had masked a region of 'negative' turbulence production but this was found not to be the case.

The dissipation rate is almost equal to the production everywhere except in the region around the velocity maximum $0{\cdot}05 < \eta < 0{\cdot}6$. This is associated with a balance of the diffusion and advection terms for $\eta > 0{\cdot}6$, and is due to the relative smallness of these terms when $\eta < 0{\cdot}05$. A similar approximate balance of diffusion and advection also seems to exist in a free jet for $\eta > 0{\cdot}6$ (Bradbury 1965), the origin for y now being the velocity maximum.

The measured diffusion due to the velocity fluctuations is quite close to the total diffusion obtained by difference. In principle the diffusion term involving the pressure fluctuations is the difference between the two but the level of precision of the measurements, particularly of the dissipation rate, renders such a result of doubtful accuracy except possibly near to the outer edge of the flow, where the dissipation and production are small. It is interesting to observe, however, that for $\eta > 0{\cdot}6$ the 'pressure' diffusion term so obtained varies in qualitatively the same way as that determined by Wygnanski & Fielder (1969) in their axisymmetric free jet.

4.7. *The Reynolds stress equations*

Assuming local isotropy the terms in the Reynolds stress equations (9) were evaluated and are shown in figures 20 (*a*)–(*d*). The terms

$$\overline{\frac{p}{\rho}\frac{\partial u}{\partial x}}, \quad \overline{\frac{p}{\rho}\frac{\partial v}{\partial y}}, \quad \overline{\frac{p}{\rho}\frac{\partial w}{\partial z}}$$

were found by difference and

$$\overline{\frac{p}{\rho}\left(\frac{\partial u}{\partial y}+\frac{\partial v}{\partial x}\right)}$$

was obtained in the same way, neglecting the diffusion term $\partial(\overline{pu}/\rho)/\partial y$. Experimental points are not shown in figure 20 because nearly all the results are derived from mean curves drawn through the data, and, in some cases, numerical differentiation of these curves. Hanjalić & Launder (1972*b*) have proposed a model for the pressure–velocity gradient correlations R and PS based on the work of Chou (1945) and Rotta (1951, 1962). The model includes the effect of the interaction between the mean rate of strain and the turbulence and for two-dimensional boundary-layer flows the following expressions are assumed for the pressure–velocity gradient correlations:

$$\overline{\frac{p}{\rho}\frac{\partial u}{\partial x}} = -C_{\phi_1}\left(\frac{\epsilon}{q^2}\right)(\overline{u^2}-\tfrac{1}{3}\overline{q^2})+\overline{uv}\frac{\partial U}{\partial y}\left(\frac{6+4C_{\phi_2}}{11}-\frac{\overline{u^2}}{\tfrac{1}{2}\overline{q^2}}C_{\phi_2}\right), \tag{22a}$$

$$\overline{\frac{p}{\rho}\frac{\partial v}{\partial y}} = -C_{\phi_1}\left(\frac{\epsilon}{q^2}\right)(\overline{v^2}-\tfrac{1}{3}\overline{q^2})-\overline{uv}\frac{\partial U}{\partial y}\left(\frac{4-12C_{\phi_2}}{11}+\frac{\overline{v^2}}{\tfrac{1}{2}\overline{q^2}}C_{\phi_2}\right), \tag{22b}$$

$$\overline{\frac{p}{\rho}\frac{\partial w}{\partial z}} = -C_{\phi_1}\left(\frac{\epsilon}{q^2}\right)(\overline{w^2}-\tfrac{1}{3}\overline{q^2})-\overline{uv}\frac{\partial U}{\partial y}\left(\frac{2-6C_{\phi_2}}{11}+\frac{\overline{w^2}}{\tfrac{1}{2}\overline{q^2}}C_{\phi_2}\right), \tag{22c}$$

$$\overline{\frac{p}{\rho}\left(\frac{\partial u}{\partial y}+\frac{\partial v}{\partial x}\right)} = -C_{\phi_1}\left(\frac{\epsilon}{q^2}\right)2\overline{uv}+\frac{\partial U}{\partial y}\left(\frac{1-3C_{\phi_2}}{55}\overline{q^2}-\frac{2-6C_{\phi_2}}{11}\overline{u^2}+\frac{8-2C_{\phi_2}}{11}\overline{v^2}-\frac{\overline{uv}^2}{\overline{q^2}}C_{\phi_2}\right), \tag{22d}$$

where C_{ϕ_1} and C_{ϕ_2} are constants given as 2·8 and 0·45 respectively. The right-hand sides of equations (22*a*) were evaluated using measured quantities, first including the term involving the mean rate of strain $\partial U/\partial y$ and then with it omitted. It can be seen in figure 20 that the model is in quite good agreement with experiment when the mean rate of strain term is included, apart from the region $\eta < 0{\cdot}3$ in the case of the normal stresses, and is significantly better than when it is not included. In order to be consistent with the level of approximation used in (9) for the Reynolds stresses equations (22*a*) should strictly include terms involving $\partial U/\partial x$ but these were found to be small and in view of the approximate nature of the model in other respects they have been omitted.

Hanjalić & Launder also proposed a model for the triple velocity correlations which occur in the diffusion terms of the Reynolds stress equations and their expressions for these can be written as

$$\overline{u^3} = -C_s \frac{\frac{3}{2}\overline{q^2}}{\epsilon} \overline{uv} \frac{\partial \overline{u^2}}{\partial y}, \tag{23a}$$

$$\overline{uv^2} = -C_s \frac{\frac{1}{2}\overline{q^2}}{\epsilon} \left(\overline{uv} \frac{\partial \overline{v^2}}{\partial y} + 2\overline{v^2} \frac{\partial \overline{uv}}{\partial y} \right), \tag{23b}$$

$$\overline{uw^2} = -C_s \frac{\frac{1}{2}\overline{q^2}}{\epsilon} \overline{uv} \frac{\partial \overline{w^2}}{\partial y}, \tag{23c}$$

$$\overline{vu^2} = -C_s \frac{\frac{3}{2}\overline{q^2}}{\epsilon} \left(\overline{v^2} \frac{\partial \overline{u^2}}{\partial y} + 2\overline{uv} \frac{\partial \overline{uv}}{\partial y} \right), \tag{23d}$$

$$\overline{v^3} = -C_s \frac{\frac{3}{2}\overline{q^2}}{\epsilon} \overline{v^2} \frac{\partial \overline{v^2}}{\partial y}, \tag{23e}$$

$$\overline{vw^2} = -C_s \frac{\frac{1}{2}\overline{q^2}}{\epsilon} \overline{v^2} \frac{\partial \overline{w^2}}{\partial y}, \tag{23f}$$

where $C_s = 0{\cdot}08$. Again using measured quantities to evaluate the right-hand sides these expressions have been compared with the measured triple velocity correlations in figure 13. In the case of $\overline{vu^2}$, $\overline{v^3}$ and $\overline{vw^2}$ the agreement is fairly good except that the model correlations reached their maximum positive values somewhat further from the wall than the measured ones. The model $\overline{u^3}$ and $\overline{uw^2}$ are too small by a factor of at least 2 but these correlations do not occur in the boundary-layer form of the Reynolds stress equations so this may not be very important. The agreement in the case of $\overline{uv^2}$ could be described as fair, the model value being too small for $\eta > 1{\cdot}0$ but close to experiment nearer to the wall.

In obtaining the simplified form of the Reynolds stress equations given by (9) it has been assumed that at high wavenumbers where nearly all the dissipation occurs the turbulence is locally isotropic. Arguments which make this a reasonable assumption for sufficiently high turbulence Reynolds number have been described by Batchelor (1953, chap. 6) in a discussion of the conditions for the existence of a range of 'universal equilibrium'. However, precisely what constitutes a sufficiently high Reynolds number has not been established largely owing to the difficulty of making accurate measurements at high wavenumbers. The turbulence Reynolds number $(\overline{u^2})^{\frac{1}{2}} \lambda/\nu$ in the outer part of the wall jet was about 400 at $x/b = 194$. This represents an improvement on the value of approximately 130 of Champagne *et al.* (1970), who also used the local-isotropy assumption in obtaining the pressure–velocity gradient correlations by difference from the Reynolds stress equations. The measurements of the latter authors indicated that the turbulence in their experiment was 'roughly isotropic' at high wavenumbers, which gives support to the use of the assumption of the local isotropy in the present case. Near to the wall, of course, the turbulence Reynolds number

becomes much smaller than in the outer region and the assumption becomes invalid.

4.8. *The position of zero shear stress*

In the present experiments the point of zero shear stress always remained closer to the wall than the velocity maximum, which is also the case for the wall jet in still air (e.g. Guitton 1970). At the velocity maximum $\overline{uv}$ has a positive value and figure 20(*d*) shows that the diffusion term in the transport equation of $\overline{uv}$ is responsible. An interpretation of this is that the diffusion of positive $\overline{uv}$ towards the velocity maximum from the outer layer dominates that of negative $\overline{uv}$ from the inner layer. The data of Erian & Eskinazi (1964) are interesting in this context because they show that in a weak wall jet this situation can be reversed. The reason for this appears to be that in a weak wall jet the turbulence level in the boundary-layer region becomes higher than in the outer region as is evident in Erian & Eskinazi's data.

5. Conclusions

The following conclusions may be drawn from the present experiments.

(*a*) It is possible to set up a wall jet in streaming flow that is closely self-preserving both in the mean flow and the turbulence.

(*b*) The mean velocity profile in the region close to the wall was logarithmic with constants which are similar to the conventional values found in boundary layers and pipe flows.

(*c*) The skin-friction formula of Bradshaw & Gee (1962) for wall jets in an external stream with a zero pressure gradient agrees well with the measured skin friction.

(*d*) The absolute values of the rates of dissipation and production of turbulent kinetic energy were almost equal except near to the velocity maximum. This observation is associated with the near cancellation of the advection and diffusion terms in the outer layer and with the smallness of these terms in the inner region.

(*e*) The production of turbulence kinetic energy did not become negative near to the velocity maximum because in this region the normal stress production term was positive and of the same order as the negative shear stress term. The point of zero shear stress was, however, always closer to the wall than the velocity maximum.

(*f*) The model proposed by Hanjalić & Launder (1972*b*) for pressure–velocity gradient correlations is in quite good agreement with experiment. The more important of the triple velocity correlations are also modelled quite well.

(*g*) The value of the constant factor in the $-\frac{5}{3}$ law for the inertial subrange was found indirectly to be 0·45.

The author would like to thank Dr B. G. Newman for many helpful discussions and Mr Lek Ah Chai for his assistance in some of the data analysis. This work was supported by the Defence Research Board of Canada under Grant number 9551-12.

REFERENCES

BATCHELOR, G. K. 1953 *The Theory of Homogeneous Turbulence.* Cambridge University Press.

BRADBURY, L. J. S. 1965 The structure of a self-preserving plane jet. *J. Fluid Mech.* **23**, 31.

BRADSHAW, P. 1963 The effect of wind tunnel screens on 'two-dimensional' boundary layers. *Nat. Phys. Lab. Aero. Rep.* no. 1085.

BRADSHAW, P. 1967 Conditions for the existence of an inertial subrange in turbulent flow. *Nat. Phys. Lab. Aero. Rep.* no. 1220.

BRADSHAW, P. & FERRISS, D. H. 1965 The spectral energy balance in a turbulence mixing layer. *Aero. Res. Counc. Current Paper,* no. 899.

BRADSHAW, P. & GEE, M. T. 1962 Turbulent wall jets with and without an external stream. *Aero. Res. Counc. R. & M.* no. 3252.

CHAMPAGNE, F. H., HARRIS, V. G. & CORRSIN, S. 1970 Experiments in nearly homogeneous turbulent shear flow. *J. Fluid Mech.* **41**, 81.

CHAMPAGNE, F. H., SLEICHER, C. A. & WEHRMANN, O. H. 1967 Turbulence measurements with inclined hot wires. Part 1. *J. Fluid Mech.* **28**, 153.

CHOU, P. Y. 1945 On velocity correlations and the solutions of the equations of turbulent fluctuation. *Quart. Appl. Math.* **3**, 38.

EAST, L. F. 1967 Measurement of skin friction at low subsonic speeds by the razor-blade technique. *Aero. Res. Counc. R. & M.* no. 3525.

ERIAN, F. & ESKINAZI, S. 1964 The wall-jet in a longitudinal pressure gradient. *Syracuse University Res. Inst., Mech. & Aerospace Engng Dept. Rep.* ME 937-6410F.

FEKETE, G. I. 1970 Two-dimensional, self-preserving turbulent jets in streaming flow. *Mech. Eng. Res. Lab., McGill University, Rep.* no. 70-11,

FOSTER, D. N., IRWIN, H. P. A. H. & WILLIAMS, B. R. 1971 The two-dimensional flow around a slotted flap. *Aero. Res. Counc. R. & M.* no. 3681.

GARTSHORE, I. S. 1965 The streamwise development of two-dimensional wall-jets and other two-dimensional turbulent shear flows. Ph.D. thesis, McGill University.

GARTSHORE, I. S. & HAWALESHKA, O. 1964 The design of a two-dimensional blowing slot and its application to a turbulent wall jet in still air. *Mech. Engng Res. Lab., McGill University, Tech. Note,* no. 64-5.

GARTSHORE, I. S. & NEWMAN, B. G. 1969 Small perturbation jets and wakes which are approximately self-preserving in a pressure gradient. *C.A.S.I. Trans.* **2**, 101.

GRANT, H. L., STEWART, R. W. & MOILLIET, A. 1962 Turbulence spectra from a tidal channel. *J. Fluid Mech.* **12**, 241.

GUITTON, D. E. 1970 Some contributions to the study of equilibrium and non-equilibrium wall jets over curved surfaces. Ph.D. thesis, McGill University.

HANJALIĆ, K. & LAUNDER, B. E. 1972*a* Fully developed asymmetric flow in a plane channel. *J. Fluid Mech.* **51**, 301.

HANJALIĆ, K. & LAUNDER, B. E. 1972*b* A Reynolds stress model of turbulence and its application to thin shear flows. *J. Fluid Mech.* **52**, 609.

IRWIN, H. P. A. H. 1972 The longitudinal cooling correction for wires inclined to the prongs and some turbulence measurements in fully developed pipe flow. *Mech. Engng Res. Lab., McGill University, Tech. Note,* no. 72-1.

JEROME, F. E., GUITTON, D. E. & PATEL, R. P. 1971 Experimental study of the thermal wake interference between closely spaced wires of a X-type hot wire. *Aero. Quart.* **22**, 119.

KACKER, S. C. & WHITELAW, J. H. 1969 The turbulence characteristics of two-dimensional wall jet and wall wake flows. *Dept. Mech. Engng, Imperial College, Rep.* BL/TN/6.

KRUKA, V. & ESKINAZI, S. 1964 The wall jet in a moving stream. *J. Fluid Mech.* **20**, 555.

MacMillan, F. A. 1956 Experiments on pitot-tubes in shear flow. *Aero. Res. Counc. R. & M.* no. 3028.

McGahan, W. A. 1965 The incompressible turbulent wall jet in an adverse pressure gradient. *Gas Turbine Lab., M.I.T., Rep.* no. 82.

Mellor, G. L. & Gibson, D. M. 1966 Equilibrium turbulent boundary layers. *J. Fluid Mech.* **24**, 225.

Newman, B. G. 1967 Turbulent jets and wakes in a pressure gradient. *Fluid Mech. Internal Flow, Gen. Motors Conf.* Elsevier

Patel, R. P. 1962 Self-preserving, two dimensional turbulent jets and wall jets in a moving stream. M.Sc. thesis, McGill University.

Patel, R. P. 1964 The effects of wind tunnel screens and honeycombs on spanwise variation of skin friction in 'two-dimensional' turbulent boundary layers. *Mech. Engng Res. Lab., McGill University, Tech. Note*, no. 64-7.

Patel, R. P. & Newman, B. G. 1961 Self-preserving, two-dimensional turbulent jets and wall jets in a moving stream. *Mech. Engng Res. Lab., McGill University, Rep.* Ae 5.

Patel, V. C. 1965 Calibration of the Preston tube and limitations on its use in pressure gradients. *J. Fluid Mech.* **23**, 185.

Pond, S., Stewart, R. W. & Burling, R. W. 1963 Turbulence spectra in the wind over waves. *J. Atmos. Sci.* **20**, 319.

Rotta, J. C. 1951 Statistiche Theorie nichthomogener Turbulenz. *Z. Phys.* **129**, 547.

Rotta, J. C. 1962 Universal aspects of the mechanism of turbulent boundary layer flow. *Progr. Aero. Sci.* **2**, 22.

Tailland, A. & Mathieu, J. 1967 Jet pariétal. *J. Mécanique*, **6**, 103.

Townsend, A. A. 1956*a* The properties of equilibrium boundary layers. *J. Fluid Mech.* **1**, 561.

Townsend, A. A. 1956*b* *The Structure of Turbulent Shear Flow.* Cambridge University Press.

Townsend, A. A. 1961 Equilibrium layers and wall turbulence. *J. Fluid Mech.* **11**, 97.

Vroomen, L. J. 1970 Data logger operating subsystem. *Mech. Engng Res. Lab., McGill University, Memo.* no. 70-1.

Wills, J. A. B. 1963 Note on a method of measuring skin friction. *Nat. Phys. Lab. Aero. Note*, no. 1011.

Wygnanski, I. & Fiedler, H. 1969 Some measurements in the self-preserving jet. *J. Fluid Mech.* **38**, 577.

Wygnanski, I. & Gartshore, I. S. 1963 General description and calibration of the McGill 17 in. × 30 in. Blower Cascade Wind Tunnel. *Mech. Engng Res. Lab., McGill University, Tech. Note*, no. 63-7.

Wyngaard, J. C. 1969 Spatial resolution of the vorticity meter and other hot-wire arrays. *J. Sci. Instrum.* **2** (2), 983.